

Virtual photon fragmentation functions

Jianwei Qiu and Xiaofei Zhang

Department of Physics and Astronomy, Iowa State University

Ames, Iowa 50011, USA

(February 9, 2001)

Abstract

We introduce operator definitions for virtual photon fragmentation functions, which are needed for reliable calculations of Drell-Yan transverse momentum (Q_T) distributions when Q_T is much larger than the invariant mass Q . We derive the evolution equations for these fragmentation functions. We calculate the leading order evolution kernels for partons to fragment into a unpolarized as well as a polarized virtual photon. We find that fragmentation functions to a longitudinally polarized virtual photon are most important at small z , and the fragmentation functions to a transversely polarized virtual photon dominate the large z region. We discuss the implications of this finding to the J/ψ mesons' polarization at large transverse momentum.

PACS Numbers: 12.38.Bx, 12.38.cy, 13.85.Qk, 14.70.Bh

arXiv:hep-ph/0101004v2 11 Feb 2001

I. INTRODUCTION

Gluon distribution plays a central role in calculating many important signatures at hadron colliders because of the dominance of gluon initiated subprocesses. A precise knowledge of the gluon distribution is absolutely vital for reliable predictions for signal as well as background cross sections [1]. A great effort has been devoted to find good physical observables for extracting information on gluon distribution [2,3].

For many years, prompt photon production has been thought as a clean signal for information on gluon distribution because its cross section at lowest order is dominated by the ‘‘Compton’’ subprocess: $g + q \rightarrow \gamma + q$, and this dominance is preserved at higher orders [4–7]. However, the theoretical and experimental complications have limited our ability to extract clean information on gluon distribution from the direct photon data [8]. At collider energies, prompt photons are observed and their cross sections are measured only if the photons are relatively isolated in phase space. Isolation is required to reduce various hadronic backgrounds. But at the same time, the cross section is no longer totally inclusive and theoretical predictions become sensitive to the isolation parameters [6,9]. In addition, phenomenological fragmentation functions are needed for including photons emerged from the long-distance fragmentation of quarks and gluons that are themselves produced at short-distance [4,7]. Our knowledge on phenomenological fragmentation functions and the theoretical uncertainties associated with the isolation prevent fully quantitative determinations of gluon distribution from the collider data on isolated photons. Although data at fixed target energies provide good information on gluon distribution at large x [10], the controversy about how much k_T -smearing is required to understand the data introduces the significant uncertainties to the gluon distributions [11,12]. As a result, all direct photon data were excluded from recent CTEQ global analyses of parton distributions [8].

Recently, Berger, Gordon, and Klasen (BGK) show that Drell-Yan transverse momentum (Q_T) distributions in hadronic collisions are dominated by partonic subprocesses initiated by incident gluons if $Q_T > Q/2$, where Q is the invariant mass of the produced lepton pairs [13]. BGK argue that Drell-Yan Q_T distribution is an advantageous source of constraints on the gluon distribution, free from the experimental and theoretical complications of photon isolation that beset studies of prompt photon production.

Other than the difference between a virtual and a real photon, Drell-Yan and prompt photon production share the same partonic subprocesses. The virtual photon produced in Drell-Yan process subsequently decays into a pair of leptons. Since we are mainly interested in the cross section at high Q_T and low Q , we ignore the Z channel contributions in this paper. If we integrate over angular dependence of the lepton pairs, the Drell-Yan massive lepton-pair production between hadron A and B can be expressed in terms of an inclusive production of a virtual photon [13]

$$\frac{d\sigma_{AB \rightarrow \ell^+ \ell^-}(Q)}{dQ^2 dQ_T^2 dy} = \left(\frac{\alpha_{em}}{3\pi Q^2} \right) \frac{d\sigma_{AB \rightarrow \gamma^*}(Q)}{dQ_T^2 dy}. \quad (1)$$

Because of the advantage of measuring the leptons, Drell-Yan massive lepton-pair production as well as the inclusive virtual photon production defined in Eq. (1) are entirely inclusive. The usual factorization theorems in Quantum Chromodynamics (QCD) should apply [14,15],

$$\frac{d\sigma_{AB\rightarrow\gamma^*(Q)}}{dQ_T^2 dy} = \sum_{a,b} \int dx_1 \phi_{a/A}(x_1, \mu) \int dx_2 \phi_{b/B}(x_2, \mu) \frac{d\hat{\sigma}_{ab\rightarrow\gamma^*(Q)}}{dQ_T^2 dy}(x_1, x_2, Q, Q_T, y; \mu) \quad (2)$$

where $\sum_{a,b}$ run over all parton flavors, the $\phi_{a/A}$ and $\phi_{b/B}$ are parton distributions, and μ represents both renormalization and factorization scale. In Eq. (2), $d\hat{\sigma}_{ab\rightarrow\gamma^*(Q)}/dQ_T^2 dy$ are short-distance partonic hard parts and perturbatively calculable to all orders in $\alpha_s(\mu)$. Similar to prompt photon production, the lowest order ‘‘Compton’’ subprocess to a virtual photon: $g+q \rightarrow \gamma^*+q$ dominates the Q_T distributions at large Q_T as long as the collision energy is high enough to overcome the phase space penalty caused by the virtual photon mass. Therefore, Drell-Yan Q_T distribution at large Q_T is an advantageous source of information on the gluon distribution [13].

When $Q_T \gg Q$, the Q_T distributions calculated order-by-order in α_s in the conventional fixed-order QCD perturbation theory receive a large logarithm, $\ln(Q_T^2/Q^2)$, at every power of α_s beyond the leading order. Therefore, at sufficiently large Q_T and \sqrt{S} , the convergence of the conventional perturbative expansion in powers of α_s is impaired, and the logarithms must be resummed.

In order to resum the large logarithm, we introduce a concept of virtual photon fragmentation functions $D_{f\rightarrow\gamma^*}(z, \mu_F; Q)$ for a parton of flavor f to fragment into a virtual photon of invariant mass Q . Normally, a virtual particle state is not physical, and therefore, a fragmentation function to such a state may be gauge dependent and ill-defined. However, if such a virtual state immediately decays into a *completely* measured physical state, we believe that a fragmentation function to such a virtual state is effectively physical. The fragmentation function is experimentally measurable if the decay to the physical state is calculable.

Unlike the real photon fragmentation functions [4], the virtual photon fragmentation functions are fully perturbative if $Q \gg \Lambda_{\text{QCD}}$. In terms of the virtual photon fragmentation functions, the conventional perturbative expansion for $d\hat{\sigma}_{ab\rightarrow\gamma^*(Q)}/dQ_T^2 dy$ in Eq. (2) can be *reorganized* according to a new factorization formula such that the large logarithms are resummed to all orders in α_s . The detailed derivation of the new factorization formula for the virtual photon production at $Q_T \geq Q$ and the discussions on the all order resummations will be published elsewhere. In this paper, we concentrate on the process independent physics associated with the virtual photon fragmentation functions.

In the next section, we derive the cut-vertex and corresponding operator definitions for virtual photon fragmentation functions. From the definitions, we derive the evolution equations (or renormalization group equations) for these fragmentation functions. We calculate the leading order evolution kernels for the evolution equations. By solving the evolution equations with the calculated evolution kernels, we derive the virtual photon fragmentation functions. We show that the virtual photon fragmentation functions are in principle perturbatively calculable to all orders in α_s if $Q \gg \Lambda_{\text{QCD}}$.

Because of our ability of measuring the leptons, we can probe the polarization of the virtual photon in Drell-Yan massive lepton-pair production. Therefore, it is also physically meaningful to define fragmentation functions to a virtual photon with a specific polarization. In Sec. III, we derive the evolution equations and the leading order evolution kernels to polarized virtual photon fragmentation functions.

In Sec. IV, we present our numerical results for virtual photon fragmentation functions. By showing the fragmentation functions at different scales, we demonstrate the evolution properties of the fragmentation functions for partons to a unpolarized as well as a polar-

ized virtual photon. We find that fragmentation functions to a longitudinally polarized virtual photon are most important at small z , and the fragmentation functions to a transversely polarized virtual photon dominate the large z region. When Q_T is large while \sqrt{S} is fixed, fragmentation functions at large z are more relevant for calculating the cross sections. Therefore, we conclude that the virtual photons produced in a unpolarized Drell-Yan massive lepton-pair production are more likely to be transversely polarized at high Q_T .

Recent data on J/ψ polarization measured by CDF collaboration at Fermilab Tevatron seem to be inconsistent with the predictions from various models of J/ψ production [16]. The virtual photon production (extracted from Drell-Yan massive lepton-pair production) at large Q_T and small Q^2 has a lot in common with the J/ψ production at high Q_T . They both have two large physical scales: Q_T and Q^2 , which is equal to $M_{J/\psi}^2$ in the case of J/ψ production; and Q_T^2 is much larger than Q^2 . If the collision energy \sqrt{S} is large enough and the logarithm $\ln(Q_T^2/Q^2)$ is so important that the resummed fragmentation contributions dominate the production cross sections, the virtual photon and J/ψ production will share the *same* partonic subprocesses. Only difference between the virtual photon and J/ψ production at high Q_T is the fragmentation functions. The virtual photon fragmentation functions are completely perturbative, while the parton to J/ψ fragmentation functions involve final-state nonperturbative interactions. Understanding the difference in such final-state interactions is very important for reliable predictions of J/ψ production. We propose to measure the virtual photon polarization in Drell-Yan massive lepton-pair production at large Q_T and low Q^2 . Because the virtual photon polarizations in Drell-Yan massive lepton-pair production are completely calculable and independent of the final-state nonperturbative effect, the measurements of the virtual photon polarizations at high Q_T provide not only a good test of QCD perturbation theory, but also a reference process to test the models of J/ψ formation.

II. UNPOLARIZED VIRTUAL PHOTON FRAGMENTATION FUNCTIONS

Like other fragmentation functions [17], a virtual photon fragmentation function, $D_{f \rightarrow \gamma^*}(z, \mu_F; Q)$ is defined as a probability density to find a virtual photon of invariant mass Q and momentum fraction z from a parent parton of flavor f . In this section, we derive the operator definitions for virtual photon fragmentation functions, and corresponding evolution equations. We calculate the leading order evolution kernels for the evolution equations and derive the virtual photon fragmentation functions by solving the evolution equations numerically.

In order to simplify our derivations, we choose a frame in which the virtual photon is moving very fast along the z -axis,

$$Q^\mu = (Q^+, Q^-, 0_T), \quad \text{and} \quad Q^- = \frac{Q^2}{2Q^+} \quad (3)$$

with $Q^+ \gg Q^-$. We also introduce two useful vectors

$$\bar{n}^\mu = (1, 0, 0_T) \quad \text{and} \quad n^\mu = (0, 1, 0_T) \quad (4)$$

with $\bar{n}^2 = n^2 = 0$ and $\bar{n}^\mu n_\mu = 1$. For any four-vector p , we have $p^\mu \bar{n}_\mu = p^-$ and $p^\mu n_\mu = p^+$.

Consider a generic quark to virtual photon fragmentation process, as shown in Fig. 1(a). The top part, labeled by T , corresponds to the fragmentation from a quark of momentum k to a virtual photon of invariant mass Q ; and the bottom part, labeled by B , represents a short-distance hard collision at a scale $\mu \gg Q$. By carrying out collinear expansion of the quark momentum k in the B at $k^\mu = (Q^+/z)\bar{n}^\mu$ and separation of the trace between the top and the bottom [18], we factorize the generic fragmentation process as follows,

$$\begin{aligned}
& \int \frac{d^4k}{(2\pi)^4} \text{Tr} [B_q(\mu, k) T_{q \rightarrow \gamma^*}(k, Q)] \\
& \approx \int \frac{dz}{z^2} \text{Tr} \left[B_q(\mu, k = \frac{Q^+}{z}) \left\{ \gamma^- \left(\frac{Q^+}{z} \right) \right\} \right] \\
& \quad \times \int \frac{d^4k}{(2\pi)^4} \text{Tr} \left[\left\{ \frac{\gamma^+}{4k^+} z^2 \delta(z - \frac{Q^+}{k^+}) \right\} T_{q \rightarrow \gamma^*}(k, Q) \right] \\
& \equiv \int \frac{dz}{z^2} H_q(\mu, k = \frac{Q^+}{z}) D_{q \rightarrow \gamma^*}(z, \mu_F; Q). \tag{5}
\end{aligned}$$

where $H_q(\mu, k = Q^+/z) \equiv \text{Tr}[B_q(\mu, k = Q^+/z)\{\gamma^-(Q^+/z)\}]$ represents the leading power short-distance production of a quark of momentum $k^\mu = (Q^+/z)\bar{n}^\mu$ and

$$D_{q \rightarrow \gamma^*}(z, \mu_F; Q) \equiv \int \frac{d^4k}{(2\pi)^4} \text{Tr} \left[\left\{ \frac{\gamma^+}{4k^+} z^2 \delta(z - \frac{Q^+}{k^+}) \right\} T_{q \rightarrow \gamma^*}(k, Q) \right] \tag{6}$$

is the quark-to-virtual-photon fragmentation function in terms of its cut-vertex definition [19]. As shown in Fig. 1(b), the $\{\frac{\gamma^+}{4k^+} z^2 \delta(z - \frac{Q^+}{k^+})\}$ in Eq. (6) is the corresponding cut-vertex. The cut-vertex for an antiquark-to-virtual-photon fragmentation function is the same as that for a quark-to-virtual-photon fragmentation function.

Similarly, by considering a generic gluon to virtual photon fragmentation process, we derive the cut-vertex definition for the gluon-to-virtual-photon fragmentation function with the cut-vertex $\{\frac{1}{2} d^{\mu\nu} z^2 \delta(z - \frac{Q^+}{k^+})\}$, as shown in Fig. 1(c). The tensor $d^{\mu\nu}$ is defined as

$$d^{\mu\nu} = -g^{\mu\nu} + \bar{n}^\mu n^\nu + n^\mu \bar{n}^\nu. \tag{7}$$

From the cut-vertex definitions in Figs. 1(b) and 1(c), we derive corresponding operator definitions for virtual photon fragmentation functions as follows. By representing the diagram in Fig. 1(b) in terms of quark fields, we have

$$\begin{aligned}
D_{q \rightarrow \gamma^*}(z, \mu_F; Q) &= \int \frac{d^4k}{(2\pi)^4} \left[z^2 \delta(z - \frac{Q^+}{k^+}) \frac{1}{4k^+} \right] (2\pi)^4 \delta^4(k - Q - \sum_X k_X) \prod_X \frac{d^3k_X}{(2\pi)^3 2E_X} \\
& \quad \times \frac{1}{N} \sum_{i=1}^N \text{Tr} \left[\gamma^+ \langle 0 | \psi_{q_i}(0) | \gamma^*(Q) X \rangle \langle X \gamma^*(Q) | \bar{\psi}_{q_i}(0) | 0 \rangle \right] \tag{8} \\
&= \frac{z}{4} \int \frac{dy^-}{2\pi} e^{-i(Q^+/z)y^-} \frac{1}{N} \sum_{i=1}^N \text{Tr} \left[\gamma^+ \langle 0 | \psi_{q_i}(0) | \gamma^*(Q) \rangle \langle \gamma^*(Q) | \bar{\psi}_{q_i}(y^-) | 0 \rangle \right].
\end{aligned}$$

where $(1/N) \sum_{i=1}^N$ with $N = 3$ indicates the average over the quark color. Similarly, we derive the operator definition for the gluon-to-virtual-photon fragmentation function,

$$\begin{aligned}
D_{g \rightarrow \gamma^*}(z, \mu_F; Q) &= \frac{z^2}{2Q^+} \int \frac{dy^-}{2\pi} e^{-i(q^+/z)y^-} (-g_{\mu\nu}) \\
&\times \frac{1}{N^2 - 1} \sum_{a=1}^{N^2-1} \langle 0 | F_a^{+\mu}(0) | \gamma^*(Q) \rangle \langle \gamma^*(Q) | F_a^{+\nu}(y^-) | 0 \rangle.
\end{aligned} \tag{9}$$

Both operator definitions in Eqs. (8) and (9) are in the light-cone gauge. Proper insertion of a line integral of the color and electromagnetic potential is needed to make them both color and electromagnetic gauge invariant [17,20].

From either the cut-vertex definitions or the operator definitions, we derive the evolution equations (or renormalization group equations) for virtual photon fragmentation functions [21],

$$\begin{aligned}
\mu_F^2 \frac{d}{d\mu_F^2} D_{c \rightarrow \gamma^*}(z, \mu_F; Q) &= \left(\frac{\alpha_{em}}{2\pi} \right) \gamma_{c \rightarrow \gamma^*}(z, \mu_F, \alpha_s; Q) \\
&+ \left(\frac{\alpha_s}{2\pi} \right) \sum_d \int_z^1 \frac{dz'}{z'} P_{c \rightarrow d}\left(\frac{z}{z'}, \alpha_s\right) D_{d \rightarrow \gamma^*}(z', \mu_F; Q),
\end{aligned} \tag{10}$$

where $c, d = q, \bar{q}, g$. The fragmentation scale μ_F is defined to be the scale where the operators of the fragmentation functions are renormalized. We choose the μ_F^2 to be the invariant mass of the fragmenting parton at the renormalization point.

The evolution kernels $\gamma_{c \rightarrow \gamma^*}$ and $P_{c \rightarrow d}$ in Eq. (10) have the following perturbative expansions,

$$\gamma_{c \rightarrow \gamma^*}(z, \mu_F, \alpha_s; Q) = \sum_{n=0} \gamma_{c \rightarrow \gamma^*}^{(n)}(z, \mu_F; Q) \left(\frac{\alpha_s}{2\pi} \right)^n, \tag{11}$$

$$P_{c \rightarrow d}(z, \alpha_s) = \sum_{n=0} P_{c \rightarrow d}^{(n)}(z) \left(\frac{\alpha_s}{2\pi} \right)^n, \tag{12}$$

where the renormalization scale dependence is suppressed. In our derivation of Eq. (10), we assume a strong ordering in partons' invariant mass in the fragmentation sequence, except the last step (quark-to-virtual photon). As a result, the evolution kernels $P_{c \rightarrow d}$ for the homogeneous terms in Eq. (10) are the same as the kernels for the DGLAP equation [22]. Although the evolution equations in Eq. (10) have the same functional form as that for real photon fragmentation functions [4], the evolution kernels $\gamma_{c \rightarrow \gamma^*}$ are different due to the nonvanish mass of the virtual photon.

In order to calculate the evolution kernels $\gamma_{c \rightarrow \gamma^*}$, we need to specify the polarization vector $\epsilon_\lambda^\mu(Q)$ for the virtual photon state $|\gamma^*(Q)\rangle$. For an unpolarized virtual photon, we need only the following polarization tensor,

$$P^{\mu\nu}(Q) \equiv \sum_{\lambda=T,L} \epsilon_\lambda^{*\mu}(Q) \epsilon_\lambda^\nu(Q), \tag{13}$$

where T and L represent the virtual photon's transverse and longitudinal polarization, respectively. Although the evolution kernels and the fragmentation functions defined in Eqs. (8) and (9) are gauge invariant, the functional form of the polarization tensor $P^{\mu\nu}(Q)$ as well as the number of Feynman diagrams contributing to the evolution kernels are gauge dependent.

In the light-cone gauge, we have the polarization tensor

$$P^{\mu\nu}(Q) = -g^{\mu\nu} + \frac{Q^\mu n^\nu + n^\mu Q^\nu}{Q \cdot n}, \quad (14)$$

and have only one Feynman diagram, as shown in Fig. 1(d), which contributes to the lowest order quark-to-virtual-photon fragmentation function. We obtain

$$D_{q \rightarrow \gamma^*}^{(0)}(z, \mu_F; Q) = e_q^2 \left(\frac{\alpha_{em}}{2\pi} \right) \left[\left(\frac{1 + (1-z)^2}{z} \right) \ln \left(\frac{z\mu_F^2}{Q^2} \right) - z \left(1 - \frac{Q^2}{z\mu_F^2} \right) \right], \quad (15)$$

where e_q is the fractional charge for the quark of flavor q , and the fragmentation scale $\mu_F^2 \geq Q^2/z$ due to the kinematics.

For an arbitrary choice of gauge, we need a total of four Feynman diagrams for the lowest order quark-to-virtual-photon fragmentation, as shown in Fig. 2 [23]. The diagrams in Fig. 2 contain double “eikonal” lines, and the Feynman rules for the double “eikonal” lines can be found in Refs. [17,23]. These four diagrams in Fig. 2 form a gauge invariant set at this order [23,24]. Contributions of the three diagrams from Figs. 2(b) to 2(d) vanish when they are contracted by the light-cone gauge polarization tensor in Eq. (14). With the covariant polarization tensor

$$P^{\mu\nu}(Q) = -g^{\mu\nu} + \frac{Q^\mu Q^\nu}{Q^2}, \quad (16)$$

or simply $P^{\mu\nu}(Q) = -g^{\mu\nu}$, we obtain the same lowest order quark-to-virtual-photon fragmentation function in Eq. (15). Since gluon does not directly couple to a photon, we have

$$D_{g \rightarrow \gamma^*}^{(0)}(z, \mu_F; Q) = 0. \quad (17)$$

By applying $\mu_F^2 d/d\mu_F^2$ to the lowest order virtual photon fragmentation functions, we obtain the lowest order evolution kernels

$$\begin{aligned} \gamma_{q \rightarrow \gamma^*}^{(0)}(z, \mu_F; Q) &= e_q^2 \left[\frac{1 + (1-z)^2}{z} - z \left(\frac{Q^2}{z\mu_F^2} \right) \right] \theta(\mu_F^2 - \frac{Q^2}{z}), \\ \gamma_{g \rightarrow \gamma^*}^{(0)}(z, \mu_F; Q) &= 0. \end{aligned} \quad (18)$$

With the lowest order evolution kernels $\gamma_{q \rightarrow \gamma^*}^{(0)}$ in Eq. (18) and $P_{c \rightarrow d}^{(0)}$ from Ref. [22], we solve the evolution equations in Eq. (10) for the unpolarized virtual photon fragmentation functions, and present the numerical results in Sec. IV.

III. POLARIZED VIRTUAL PHOTON FRAGMENTATION FUNCTIONS

By measuring the momenta of both leptons in Drell-Yan massive lepton-pair production, we can determine both invariant mass and polarization state of the virtual photon, which decays into the lepton-pair. Therefore, it is meaningful to define the fragmentation functions to a polarized virtual photon. In this section, we calculate the evolution kernels for the evolution equations of polarized virtual photon fragmentation functions.

Since we did not use any constraints due to the virtual photon's polarization when we derived the cut-vertex and operator definitions for the virtual photon fragmentation functions in last section, the same definitions should be valid for fragmentation functions to a polarized virtual photon. Therefore, with a proper choice of polarization vectors $\epsilon_\lambda^\mu(Q)$ for a virtual photon of polarization λ , we can calculate the fragmentation functions to a virtual photon of a specific polarization state.

In order to specify a polarized virtual photon state, we need to define the photon's polarization vector $\epsilon_\lambda^\mu(Q)$. If the photon is real ($Q^2 = 0$), it has only *two* transverse polarization states and its longitudinal polarization can be gauged away by an extra gauge transformation. When the photon is virtual and its quantum numbers are completely fixed by the physical observables, the extra gauge degree of freedom used to remove the longitudinal polarization at $Q^2 = 0$ is lost, and therefore, the virtual photon has three polarization states.

With our choice of the frame in which the virtual photon is moving very fast along the z -axis, we define the photon's polarization vectors as the following,

$$\begin{aligned}\epsilon_{T=1}^\mu(Q) &= (0, 1, 0, 0), \\ \epsilon_{T=2}^\mu(Q) &= (0, 0, 1, 0), \\ \epsilon_L^\mu(Q) &= \frac{1}{\sqrt{2}}([Q^+ - Q^-], 0, 0, [Q^+ + Q^-]),\end{aligned}\tag{19}$$

which are effectively the same as those in the ‘‘S-helicity’’ frame defined in Ref. [25]. We obtain corresponding polarization tensors,

$$P_T^{\mu\nu}(Q) \equiv \frac{1}{2} \sum_{T=1,2} \epsilon_T^{*\mu}(Q) \epsilon_T^\nu(Q) = \frac{1}{2} d^{\mu\nu}\tag{20}$$

with $d^{\mu\nu}$ defined in Eq. (7) and

$$P_L^{\mu\nu}(Q) \equiv \epsilon_L^{*\mu}(Q) \epsilon_L^\nu(Q)\tag{21}$$

for transversely and longitudinally polarized virtual photons, respectively. By summing over all polarization states, we should recover the polarization tensor for a unpolarized virtual photon,

$$P^{\mu\nu}(Q) = 2 P_T^{\mu\nu}(Q) + P_L^{\mu\nu}(Q),\tag{22}$$

where the factor of two represents the virtual photon's two transverse polarization states.

Applying the transverse polarization tensor $P_T^{\mu\nu}$ to the lowest order Feynman diagrams in Fig. 2, we obtain the lowest order fragmentation function for a quark to a transversely polarized virtual photon as

$$D_{q \rightarrow \gamma_T^*}^{(0)}(z, \mu_F; Q) = e_q^2 \left(\frac{\alpha_{em}}{2\pi} \right) \frac{1}{2} \left(\frac{1 + (1-z)^2}{z} \right) \left[\ln \left(\frac{z\mu_F^2}{Q^2} \right) - \left(1 - \frac{Q^2}{z\mu_F^2} \right) \right]\tag{23}$$

with $\mu_F^2 \geq Q^2/z$. Again, the lowest order fragmentation function for a gluon to a photon vanishes, $D_{g \rightarrow \gamma_T^*}^{(0)}(z, \mu_F; Q) = 0$. Corresponding evolution kernels are given by

$$\begin{aligned}
\gamma_{q \rightarrow \gamma_T^*}^{(0)}(z, \mu_F; Q) &= e_q^2 \frac{1}{2} \left(\frac{1 + (1-z)^2}{z} \right) \left[1 - \frac{Q^2}{z\mu_F^2} \right] \theta(\mu_F^2 - \frac{Q^2}{z}), \\
\gamma_{g \rightarrow \gamma_T^*}^{(0)}(z, \mu_F; Q) &= 0.
\end{aligned} \tag{24}$$

As expected, when $Q \rightarrow 0$, $2\gamma_{q \rightarrow \gamma_T^*}^{(0)}$ in Eq. (24) reduces to the lowest order evolution kernels for the real photon fragmentation functions [4].

Similarly, by applying the longitudinal polarization tensor $P_L^{\mu\nu}$ in Eq. (21) to the Feynman diagrams in Fig. 2, we derive

$$D_{q \rightarrow \gamma_L^*}^{(0)}(z, \mu_F; Q) = e_q^2 \left(\frac{\alpha_{em}}{2\pi} \right) \left[2 \left(\frac{1-z}{z} \right) \right] \left(1 - \frac{Q^2}{z\mu_F^2} \right), \tag{25}$$

with $\mu_F^2 \geq Q^2/z$, and $D_{g \rightarrow \gamma_L^*}^{(0)}(z, \mu_F; Q) = 0$. Our lowest order fragmentation function to a longitudinally polarized virtual photon in Eq. (25) is consistent with the result derived by Braaten and Lee [24]. The $(1-z)$ factor in Eq. (25) is a consequence of the vector interaction between the quark and photon. As a consistency check, our lowest order polarized virtual photon fragmentation functions in Eqs. (23) and (25) satisfy

$$2 D_{q \rightarrow \gamma_T^*}^{(0)}(z, \mu_F; Q) + D_{q \rightarrow \gamma_L^*}^{(0)}(z, \mu_F; Q) = D_{q \rightarrow \gamma^*}^{(0)}(z, \mu_F; Q), \tag{26}$$

where $D_{q \rightarrow \gamma^*}^{(0)}$ is given in Eq. (15). From Eq. (25), we derive the evolution kernels for longitudinally polarized virtual photon fragmentation functions

$$\begin{aligned}
\gamma_{q \rightarrow \gamma_L^*}^{(0)}(z, \mu_F; Q) &= e_q^2 \left[2 \left(\frac{1-z}{z} \right) \right] \left(\frac{Q^2}{z\mu_F^2} \right) \theta(\mu_F^2 - \frac{Q^2}{z}), \\
\gamma_{g \rightarrow \gamma_L^*}^{(0)}(z, \mu_F; Q) &= 0.
\end{aligned} \tag{27}$$

Again, we have $2\gamma_{q \rightarrow \gamma_T^*}^{(0)} + \gamma_{q \rightarrow \gamma_L^*}^{(0)} = \gamma_{q \rightarrow \gamma^*}^{(0)}$.

Since the polarized evolution kernels and the polarized virtual photon fragmentation functions are gauge invariant, we can also derive them from the single diagram in Fig. 1(d) in the light-cone gauge. Substituting $Q^\mu = Q^+ \bar{n}^\mu + Q^- n^\mu$ into the polarization tensor in the light-cone gauge in Eq. (14), we obtain

$$P^{\mu\nu}(Q) = d^{\mu\nu} + \frac{Q^2}{(Q^+)^2} n^\mu n^\nu. \tag{28}$$

Since the vector n^μ used to fix the light-cone gauge does not have transverse component, the $d^{\mu\nu}$ in Eq. (28) should still be identified as $2P_T^{\mu\nu}(Q)$. From Eq. (22), we obtain the polarization tensor for a longitudinally polarized virtual photon

$$P_L^{\mu\nu}(Q) = \frac{Q^2}{(Q^+)^2} n^\mu n^\nu \tag{29}$$

in the light-cone gauge. Applying this $P_L^{\mu\nu}(Q)$ to the Feynman diagram in Fig. 1(d), we can derive the lowest order fragmentation functions to a longitudinally polarized virtual photon. As expected, the derived fragmentation functions are the same as those given in Eq. (25).

Since the fragmentation functions to a polarized and a unpolarized virtual photon share the same form of the operator definitions, the evolution equations for polarized virtual photon fragmentation functions have the same functional form as that in Eq. (10), except the evolution kernels $\gamma_{c\rightarrow\gamma^*}$ are replaced by those in Eq. (24) and Eq. (27) for transversely polarized and longitudinally polarized virtual photon, respectively. Since the evolution kernels $P_{c\rightarrow d}$ are independent of the polarization of the produced virtual photon, they should remain the same.

IV. NUMERICAL RESULTS AND CONCLUSIONS

In last two sections, we derived the analytical expressions for the lowest order parton-to-virtual-photon fragmentation functions with the virtual photon unpolarized as well as polarized. The lowest order gluon-to-virtual-photon fragmentation functions vanish while the lowest order quark-to-virtual-photon fragmentation functions are given in Eqs. (15), (23), and (25) for unpolarized, transversely polarized, and longitudinally polarized, respectively. Strong interactions in the top blob of the cut-vertex diagrams in Figs. 1(b) and 1(c) can change the z as well as the μ_F dependence of the lowest order virtual photon fragmentation functions. Solving the evolution equations in Eq. (10) is effectively to resum all leading logarithmic contributions from the strong interactions. The power corrections from the strong interactions $O(\Lambda_{\text{QCD}}^2/\mu_F^2)$ are not included in the evolution equations.

In order to solve the evolution equations in Eq. (10), we need to specify a boundary condition. Unlike the real photon fragmentation functions, we do not need any nonperturbative input distributions if the invariant mass $Q \gg \Lambda_{\text{QCD}}$. From the pure kinematics, we have the following boundary condition for solving the evolution equations in Eq. (10),

$$D_{f\rightarrow\gamma^*}(z, \mu_F^2 \leq Q^2/z; Q) = 0 \quad (30)$$

for all parton flavor $f = q, \bar{q}, g$ and any polarization of the virtual photon.

Since the boundary conditions given in Eq. (30) are the same for all flavors of massless partons, and the evolution kernels $\gamma_{c\rightarrow\gamma^*}$ in Eq. (10) are the same for a quark q and corresponding antiquark \bar{q} , we have

$$D_{q\rightarrow\gamma^*}(z, \mu_F; Q) = D_{\bar{q}\rightarrow\gamma^*}(z, \mu_F; Q) \quad (31)$$

for all quark flavor q . By neglecting the quark mass difference, the only flavor dependence of the evolution kernels $\gamma_{c\rightarrow\gamma^*}$ in Eq. (10) is from quark's fractional charge e_q . Therefore, quark-to-virtual-photon fragmentation functions are the same for all quark flavors with the same fractional charge.

With the boundary condition given in Eq. (30), we can solve the evolution equations in Eq. (10) in the moment-space analytically, and then, perform the Mellin transformation from the moment-space back to the z -space [4]. However, we find that it is easier to solve the evolution equations numerically in the z -space directly.

In Figs. 3(a) and 3(b), we plot the derived lowest order quark-to-virtual-photon fragmentation functions as a function of the momentum fraction z at a fragmentation scale $\mu_F = 10$ GeV and $\mu_F = 50$ GeV, respectively. We choose $e_q = 2/3$ for the quark's fractional

charge, and the virtual photon's invariant mass to be $Q = 5$ GeV. The unpolarized quark-to-virtual-photon fragmentation functions given in Eq. (15) are represented by the solid lines. The transversely and longitudinally polarized virtual photon fragmentation functions given in Eqs. (23) and (25) are represented by the dashed and dotted lines, respectively. The solid lines are equal to twice of the dashed lines plus the dotted lines. which is a consequence of Eq. (26).

From Fig. 3, we find that longitudinally polarized virtual photon fragmentation functions are much larger than the transversely polarized virtual photon fragmentation functions when z is small. The small z region corresponds to the region where μ_F^2 is close to the threshold Q^2/z . Near the threshold, the evolution kernels for the transversely polarized fragmentation functions $\gamma_{q \rightarrow \gamma_T^*}(0)$ in Eq. (24) vanish while the kernels for the longitudinally polarized fragmentation functions $\gamma_{q \rightarrow \gamma_L^*}^{(0)}$ in Eq. (27) are finite and large. The $\gamma_{q \rightarrow \gamma_L^*}^{(0)}$ are actually proportional to $1/z$ when $\mu_F^2 \rightarrow Q^2/z$. Therefore, the longitudinally polarized virtual photon fragmentation functions dominate the small z or the threshold region.

On the other hand, the fragmentation functions for a transversely polarized virtual photon evolve much faster than the longitudinally polarized fragmentation functions in the large z region, as shown in Fig. 3. This is because the evolution kernels $\gamma_{q \rightarrow \gamma_L^*}^{(0)}$ for the longitudinally polarized virtual photon fragmentation functions are power suppressed (proportional to $1/\mu_F^2$) and also vanish as $z \rightarrow 1$.

In order to see the effect of resumming the large logarithms from quark and gluon radiations, we numerically solve the evolution equations in Eq. (10) with the lowest order evolution kernels $\gamma_{q \rightarrow \gamma^*}^{(0)}$ and $P_{c \rightarrow d}^{(0)}$. We plot the comparison between the lowest order (dashed) and the QCD evolved (solid) quark-to-virtual-photon fragmentation functions at $Q = 5$ GeV and $\mu_F = 50$ GeV in Fig. 4(a). The symbols: U, T, and L represent the fragmentation functions to a unpolarized, transversely polarized, and longitudinally polarized virtual photon, respectively. Like the evolution of parton distributions, QCD evolution tries to enlarge the fragmentation functions in the small z region, and to suppress the fragmentation functions in the large z region. The difference between the QCD evolved and lowest order fragmentation functions at $Q = 5$ GeV is small because of the boundary conditions in Eq. (30). However, when Q is smaller or μ_F is larger, we expect QCD evolution to be much more important because of a larger logarithm $\ln(\mu_F^2/Q^2)$. For example, cross sections for virtual photon production were measured by UA1 Collaboration at CERN for the virtual photon mass $Q \in [2m_\mu, 2.5]$ GeV [26]. Instead of $Q = 5$ GeV in Fig. 4(a), we plot the same quark-to-virtual-photon fragmentation functions at $Q = 1.5$ GeV in Fig. 4(b). Clearly, QCD evolved virtual photon fragmentation functions in Fig. 4(b) are enhanced in comparison with those in Fig. 4(a), particularly, in the small z region.

Although we do not have the lowest order gluon-to-virtual-photon fragmentation functions due to $\gamma_{g \rightarrow \gamma^*}^{(0)} = 0$, QCD evolution in Eq. (10) can generate the gluon-to-virtual-photon fragmentation functions. In Figs. 5(a) and 5(b), we plot gluon-to-virtual-photon fragmentation functions at $\mu_F = 10$ GeV and $\mu_F = 50$ GeV, respectively. The virtual photon mass is again chosen to be $Q = 5$ GeV. As shown in Fig. 5, QCD evolution generated gluon-to-virtual-photon fragmentation functions at $Q = 5$ GeV grow very fast when the fragmentation scale μ_F^2 increases. They are about two orders of magnitude smaller than the quark-to-virtual-photon fragmentation functions at $\mu_F = 10$ GeV, and only one order of magnitude smaller at $\mu_F = 50$ GeV. Therefore, at $Q = 1.5$ GeV or at a larger value of μ_F ,

QCD generated gluon-to-virtual-photon fragmentation functions become more important.

In conclusion, we have argued that virtual photon fragmentation functions are well-defined and physically meaningful. We derive the evolution equations for virtual photon fragmentation functions, and show that these fragmentation functions are perturbatively calculable. We demonstrate that QCD resummation of the large logarithms caused by quark and gluon radiation provides a very important contribution to the fragmentation functions when the fragmentation scale μ_F is large and/or the invariant mass Q is relatively small. Just like pion fragmentation functions [4], the virtual photon fragmentation functions derived here are universal and can be applied to any processes with massive lepton-pair production. In the rest of this paper, we discuss some potential applications of our results.

Contributions of fragmentation functions $D(z)$ to the physical observables generally depend on the production of the parent partons at the same z . Since the cross sections for producing the parent partons strongly depend on the momenta of the produced partons, the role of the fragmentation functions may be different for different regions of the z values. For example, for the Drell-Yan production, if the cross section is dominated by the small z region, the produced virtual photons will likely be longitudinally polarized. On the other hand, if the cross section is dominated by the large z region, the virtual photon will be transversely polarized. For a fixed collision energy \sqrt{S} , the Drell-Yan cross sections depend on the z -value from $z_{min} = \sqrt{(Q^2 + Q_T^2)/S} [e^y + e^{-y}]$ to 1 with the rapidity y . For $Q = 5$ GeV and $y = 0$ at $\sqrt{S} = 2$ TeV (the new Tevatron energy), $z_{min} \approx 0.01$ and 0.05 for $Q_T = 10$ and 50 GeV, respectively. It is clear from Fig. 3(b) that the produced virtual photons at $Q_T \sim 50$ GeV are more likely to be transversely polarized. At $Q_T = 10$ GeV, the longitudinally polarized fragmentation functions in Fig. 3(a) are much larger than the transverse fragmentation functions in small z region, and the $1/z^2$ factor in Eq. (5) for the convolution over z is also favor for producing a longitudinally polarized virtual photon. But, the cross section for producing a parent parton of momentum k_T at small $z \approx Q_T/k_T$ is a very steep falling function of k_T , and consequently, it strongly reduces the rate for producing a longitudinally polarized virtual photon. In conclusion, when Q_T is large, the virtual photon produced in Drell-Yan massive lepton-pair production is more likely to be transversely polarized.

Recently, it was found that the J/ψ mesons produced at Fermilab Tevatron become more longitudinally polarized as the transverse momentum increases [16]. On the other hand, various theoretical calculations predict the J/ψ mesons to be more transversely polarized [27]. The virtual photon production (extracted from Drell-Yan massive lepton-pair production) at large Q_T and small Q^2 has a lot in common with the J/ψ production at high Q_T . They both have two large physical scales: Q_T and Q^2 , which is equal to $M_{J/\psi}^2$ in the case of J/ψ production; and Q_T^2 is much larger than Q^2 . If the collision energy \sqrt{S} is large enough and the logarithm $\ln(Q_T^2/Q^2)$ is so important that the resummed fragmentation contributions dominate the production cross sections, the virtual photon and J/ψ production will share the *same* partonic subprocesses, labeled by the R in Fig. 6. With their respected fragmentation functions, both the virtual photon and J/ψ production at high Q_T are perturbatively calculable [28]. As discussed above, the virtual photon fragmentation functions are completely perturbative, while the parton to J/ψ fragmentation functions involve final-state nonperturbative interactions. Therefore, only difference between the virtual photon and J/ψ production at high Q_T and large \sqrt{S} is the final-state strong interactions during

the formation of J/ψ meson. We propose to measure the virtual photon polarization in Drell-Yan massive lepton-pair production at large Q_T and low Q^2 . The measurements of the virtual photon's polarization at high Q_T provide not only a good test of QCD perturbation theory, but also a reference process to test the models of J/ψ formation.

As shown in Fig. 6, the fragmentation functions from a parton d to a physical J/ψ can be approximated by the fragmentation functions to a virtual gluon of invariant mass Q , which immediately decay into a $c\bar{c}$ -pair, convoluted with a transition from the $c\bar{c}$ -pair to a physical J/ψ [28]. The fragmentation functions for a parton to a virtual gluon should be perturbatively calculable, and their dependence on the polarization should be very similar to that of the virtual photon fragmentation functions. But, the produced charm and anticharm quark pair of invariant mass Q can in principle radiate gluons and have soft interactions with other partons in the collisions. However, due to the heavy quark mass, such final-state interactions during the formation or transition from the produced $c\bar{c}$ -pair to a physical J/ψ meson are not expected to significantly change the polarization [27]. If the formation from the $c\bar{c}$ -pair of invariant mass Q to a physical J/ψ meson does not change the polarization, one can expect the polarization of the J/ψ mesons produced at high Q_T to be similar to the polarization of the virtual photon in Drell-Yan massive lepton-pair production at the same kinematics. For example, the non-relativistic QCD (NRQCD) model of J/ψ production predicts the J/ψ mesons to be transversely polarized at large transverse momentum [27], which is not consistent with recent Fermilab data [16]. Since the leptons do not interact strongly once produced, the measurements of the virtual photon polarization in Drell-Yan massive lepton-pair production at large transverse momentum should help us to narrow the questions about J/ψ production.

ACKNOWLEDGMENT

We thank G. Sterman for very helpful discussions. This work was supported in part by the U.S. Department of Energy under Grant No. DE-FG02-87ER40731.

REFERENCES

- [1] J. Huston *et al.*, Phys. Rev. **D58**, 114034 (1998).
- [2] L. de Barbaro *et al.*, hep-ph/0006300; and references therein.
- [3] S. Catani *et al.*, hep-ph/0005025; and references therein.
- [4] J.F. Owens, Rev. Mod. Phys. **59**, 465 (1987).
- [5] H. Baer, J. Ohnemus, and J.F. Owens, Phys. Rev. **D42**, 61 (1990).
- [6] E.L. Berger and J.-W. Qiu, Phys. Lett. **B248**, 371,(1990); Phys. Rev. **D44**, 2002 (1991).
- [7] P. Aurenche, R. Baier, M. Fontannaz, Phys. Rev. **D42**, 1440 (1990); P. Aurenche *et al.*, Nucl. Phys. **B399**, 34 (1993).
- [8] H.L. Lai *et al.*, Eur. Phys. J. **C12**, 375, (2000).
- [9] E.L. Berger, X.-F. Guo, and J.-W. Qiu, Phys. Rev. Lett. **76**, 2234 (1996); Phys. Rev. **D54**, 5470, (1996).
- [10] A.D. Martin, R.G. Roberts, W.J. Stirling, and R.S. Thorne, Eur. Phys. J. **C4**, 463, (1998).
- [11] L. Apanasevich *et al.*, Phys. Rev. **D 59**, 074007 (1999).
- [12] P. Aurenche *et al.*, Eur. Phys. J. **C9**, 107 (1999).
- [13] E.L. Berger, L.E. Gordon, and M. Klasen, Phys. Rev. **D58**, 074012 (1998).
- [14] J.C. Collins, D.E. Soper, and G. Sterman, in *Perturbative Quantum Chromodynamics*, edited by A. H. Mueller (World Scientific, Singapore, 1989).
- [15] G.T. Bodwin, Phys. Rev. **D31**, 2616 (1985); **D34**, 3932 (1986).
- [16] T. Affolder *et al.*, CDF Collaboration, Phys. Rev. Lett. **85**, 2886, (2000).
- [17] J.C. Collins and D.E. Soper, Nucl. Phys. **B194**, 445 (1982).
- [18] J. Qiu, Phys. Rev. **D42**, 30 (1990).
- [19] A.H. Mueller, Phys. Rep. **73**, 237, (1981).
- [20] We thank E. Braaten for pointing out the missing QED phase in an early preprint of this paper.
- [21] J.C. Collins and J.-W. Qiu, Phys. Rev. **D39**, 1398 (1989).
- [22] G. Sterman *et al.*, Rev. Mod. Phys. **67**, 157 (1995), and references therein.
- [23] G.T. Bodwin and J.-W. Qiu, Phys. Rev. **D41**, 2755 (1990).
- [24] E. Braaten and J. Lee, private communication.
- [25] C.S. Lam and W.-K. Tung, Phys. Rev. **D18**, 2447 (1978).
- [26] C. Albajar *et al.*, UA1 Collaboration, Phys. Lett. **B209**, 397 (1988).
- [27] E. Braaten, B.A. Kniehl, and J. Lee, Phys. Rev. **D62**, 094005 (2000); and references therein.
- [28] J.-W. Qiu and G. Sterman, in preparation.

FIGURES

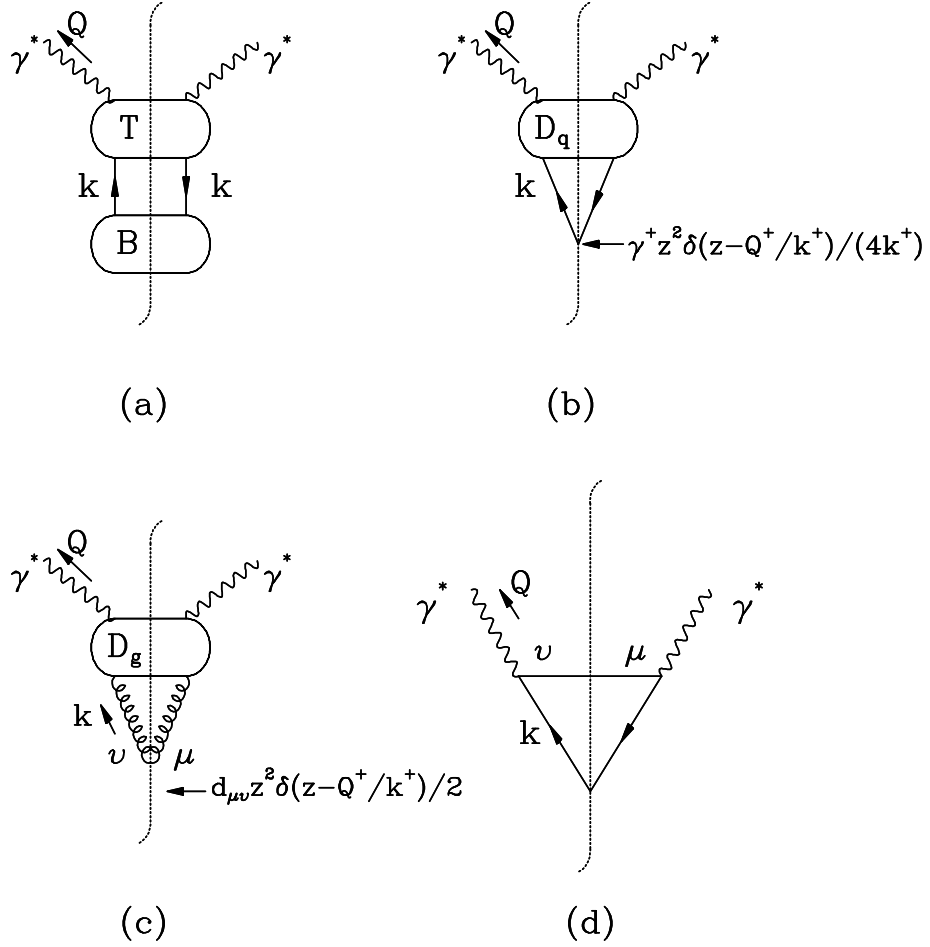


FIG. 1. (a) A generic diagram for a scattering process in which a quark of momentum k fragments into a virtual photon of invariant mass Q ; (b) the cut-vertex diagram for quark-to-virtual-photon fragmentation function; (c) the cut-vertex diagram for gluon-to-virtual-photon fragmentation function; (d) the lowest order cut-vertex diagram for a quark to a virtual photon.

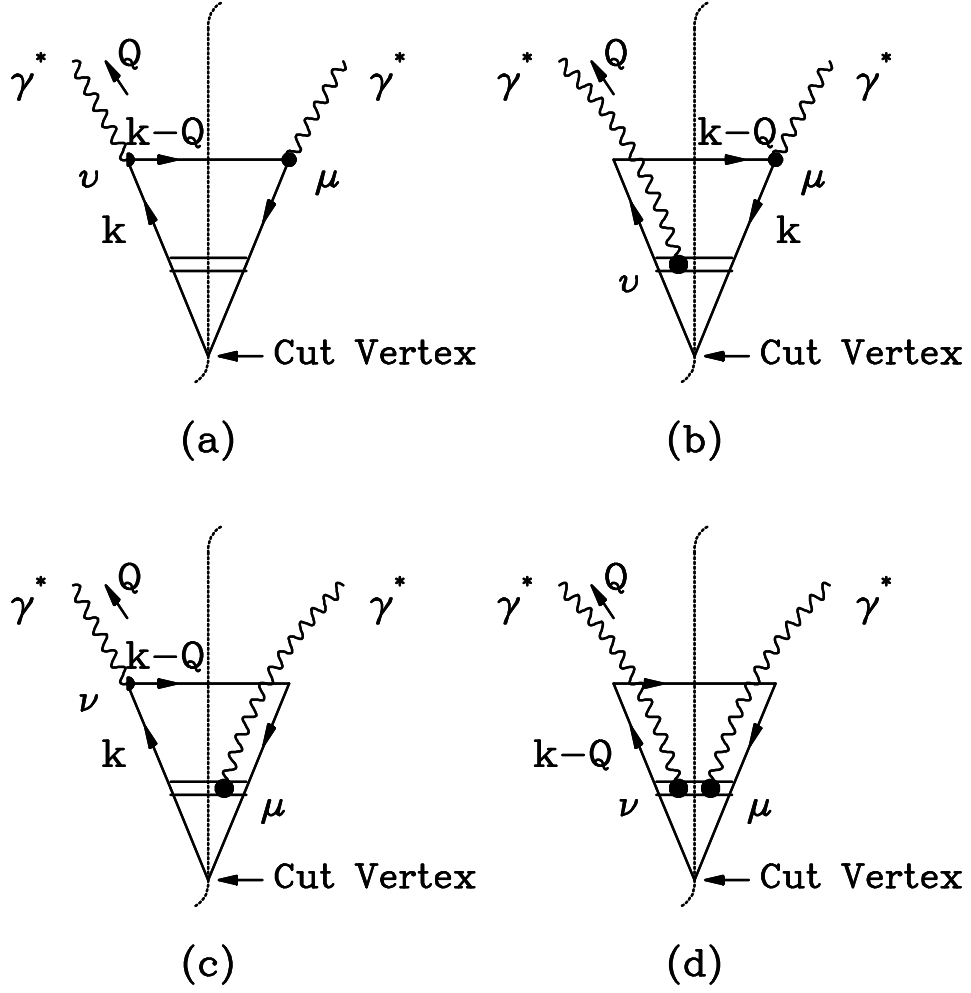


FIG. 2. Lowest order gauge invariant set of Feynman diagrams for quark-to-virtual-photon fragmentation functions [23].

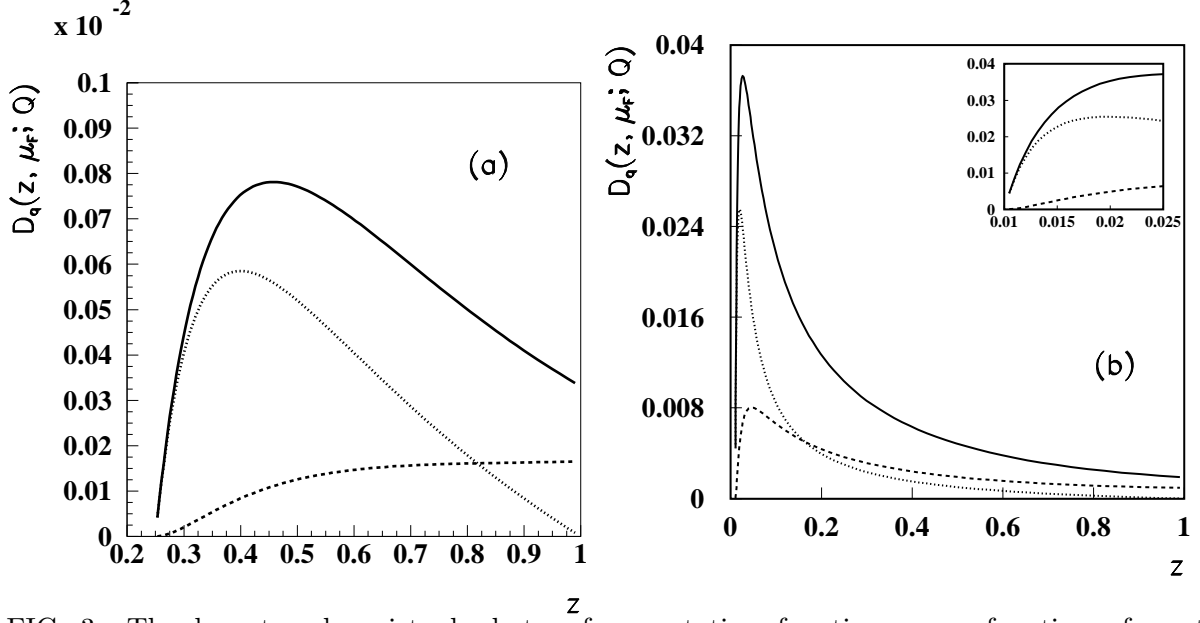


FIG. 3. The lowest order virtual photon fragmentation functions as a function of z at $Q = 5$ GeV and $\mu_F = 10$ GeV (a), and $\mu_F = 50$ GeV (b). The solid, dashed, and dotted lines are for unpolarized, transversely polarized, and longitudinally polarized virtual photons, respectively. The inset in Fig. 2(b) shows the $z \leq 0.025$ region.

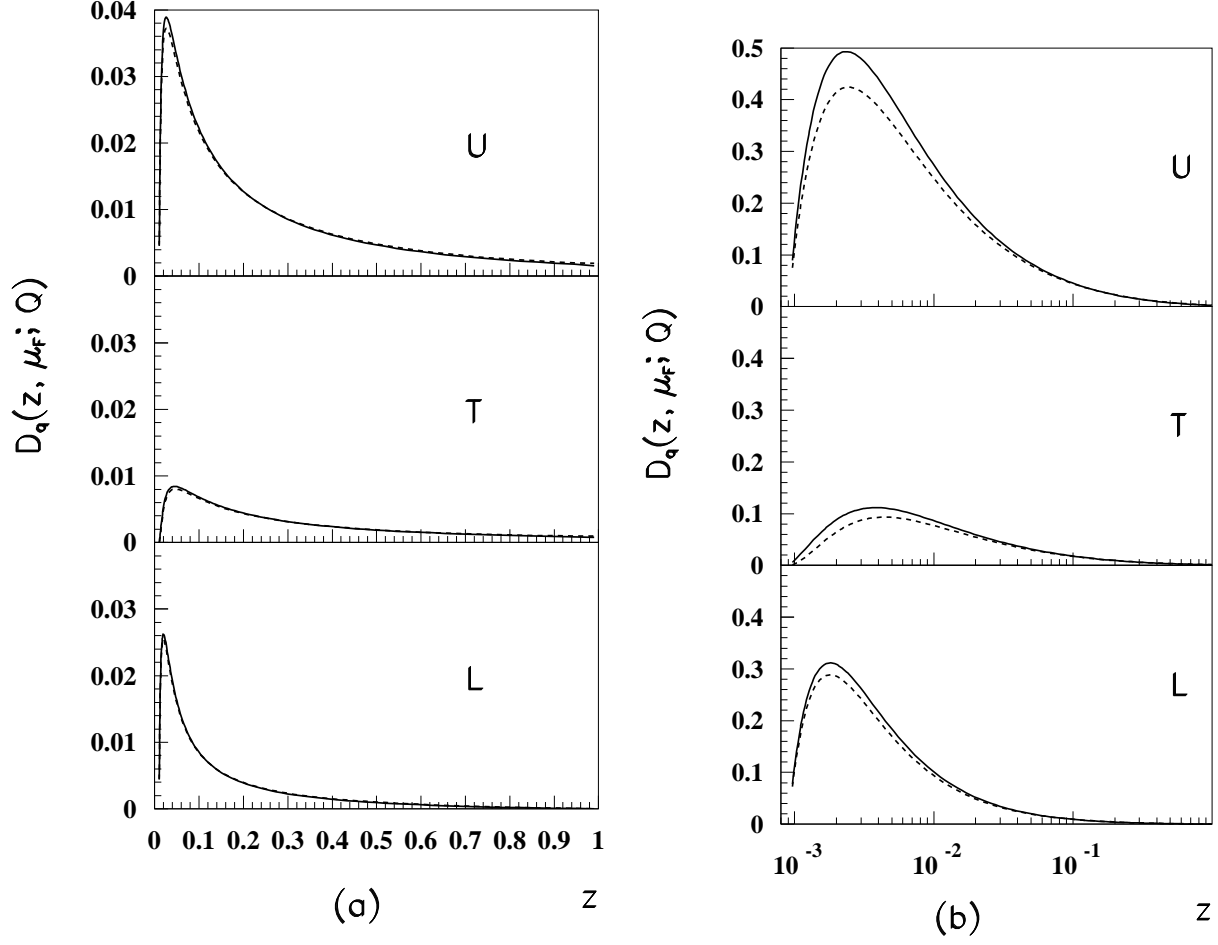


FIG. 4. Comparison between the lowest order (dashed) and the QCD evolved (solid) virtual photon fragmentation functions as a function of z at $\mu_F = 50$ GeV and $Q = 5$ GeV (a) and $Q = 1.5$ GeV (b).

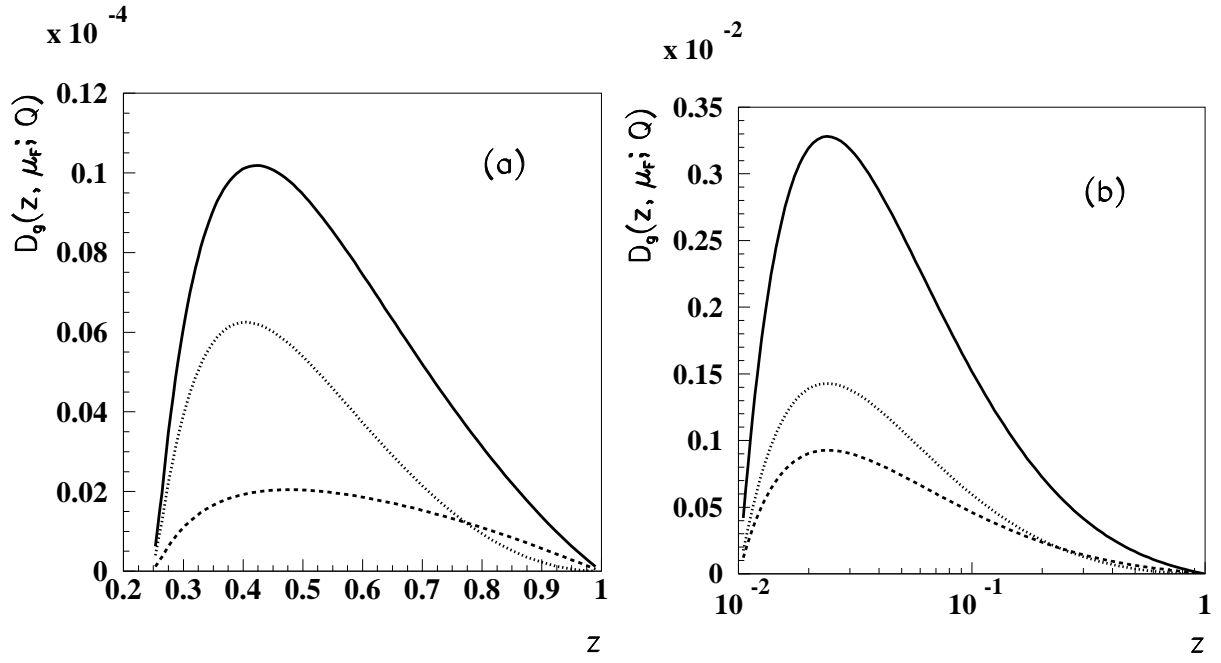


FIG. 5. QCD generated gluon-to-virtual-photon fragmentation functions as a function of z at $Q = 5$ GeV and $\mu_F = 10$ GeV (a), and $\mu_F = 50$ GeV (b). The solid, dashed, and dotted lines are for unpolarized, transversely polarized, and longitudinally polarized virtual photons, respectively.

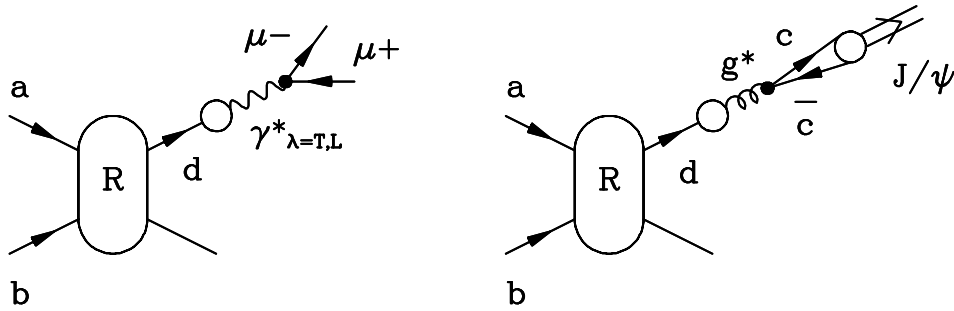


FIG. 6. Sketch for Drell-Yan massive lepton-pair and J/ψ production via parton fragmentation.